Hindawi
Advances in Materials Science and Engineering
Volume 2022, Article ID 8047519, 12 pages
https://doi.org/10.1155/2022/8047519

Research Article

Pullout Characteristics and Damage Softening Model of the Geogrid-Soil Interface

Xiaoyong Liang,[1,2,3] Jing Jin ,[2,3,4] Guangqing Yang,[4,5] Xizhao Wang,[2] and Yitao Zhou[3]

[1]*School of Traffic and Transportation, Shijiazhuang Tiedao University, Shijiazhuang 050043, China*
[2]*School of Civil Engineering, Hebei University of Science and Technology, Shijiazhuang, Hebei 050018, China*
[3]*Hebei Key Laboratory of Geotechnical Engineering Safety and Deformation Control, Hebei University of Water Resources and Electric Engineering, Cangzhou 061001, China*
[4]*State Key Laboratory of Mechanical Behavior and System Safety of Traffic Engineering Structures, Shijiazhuang Tiedao University, Shijiazhuang, Hebei 050043, China*
[5]*School of Civil Engineering, Shijiazhuang Tiedao University, Shijiazhuang, Hebei 050043, China*

Correspondence should be addressed to Jing Jin; jinjing@hebust.edu.cn

Received 22 February 2022; Revised 6 April 2022; Accepted 7 April 2022; Published 9 May 2022

Academic Editor: Ivan Giorgio

The mechanical properties of geogrid-soil interface is very important in design and stability analysis of reinforced soil structure. In order to study the complicated mechanism of geogrid-soil interface, a series of pullout tests of HDPE uniaxial tensile geogrids with the different transverse ribs spacing is used to investigate the interaction characteristics in the laboratory. The test results show that pullout force and displacement curves are characterized as strain softening; compared with the no-reinforced case, the case reinforced with geogrid has larger cohesion and lower friction angles. The ductility of soil is enhanced due to geogrid reinforcement. Based on the basic control equations of the interface and damage theory, trilinear shear stress-displacement damage softening model is proposed to describe the strain-softening characteristics of geogrid-soil interface. Analytical solutions of interface tension, shear stress, and displacement at different stages are derived considering strain softening based on damage, and the development of shear stress and progressive failure mode of the geogrid-soil interface at different pullout stages is revealed. Furthermore, the proposed model is verified by experimental results.

1. Introduction

As an important reinforced material, geogrid has been widely used in various geotechnical engineering, such as improving the structural stability of retaining wall, improving the bearing capacity of foundation, and dealing with the differential settlement between the old and the new subgrade. The reinforcement of geogrid is realized by the interaction between geogrid and surrounding soil. Therefore, the behavior of reinforcement soil interface is an important factor affecting the reinforcement mechanism of geogrid. There are still some deficiencies in the design method of geogrid reinforced soil structure. The main problem is that the understanding of the mechanism of reinforcement soil interface is not comprehensive enough. Scholars have carried out a lot of relevant experimental research work [1], such as direct shear test [2–5], triaxial compression test [6, 7], biaxial compression test [8], and pullout test [9]. The geogrid pullout test has been regarded as a simple and direct way to investigate the geogrid-soil interface behavior among all the experimental approaches.

Yang et al. [10] carried out pullout tests of geogrids with different stiffnesses in gravel and clay and discussed the influence of geogrid stiffness and soil type on the friction characteristics of reinforcement soil interface. Wang et al. [11] studied the influence of various test factors on the pullout behavior of reinforced soil interface. Xiao et al. [12] analyzed the influence of interface normal stress and

cohesive water content on the interface interaction characteristics in the pullout test. Cao et al. and Zheng et al. [13, 14] took three-dimensional geogrid as the research object and, through the indoor pullout test, studied the interaction characteristics of reinforcement soil interface and the deformation of geogrid. Jin [15] studied the influence of geogrid transverse rib spacing on the pullout test results. Abdi et al. [16] analyzed the interface parameters between geogrid and various kinds of filling through the pullout test. Wang et al. [17] analyzed the relationship between maximum pullout force and displacement through the pullout test and Fourier series approximation method. Alagiyawanna et al. [18] studied the contribution and effect of transverse rib and longitudinal rib on pullout resistance through the number of longitudinal rib and transverse rib in the pullout test. The research results of Moraci et al. [19] show that the passive resistance of transverse rib bears more than 75% of the pullout force. Cardile et al. [20] proposed a method to determine the pullout force of geogrids in sand considering the interaction between transverse ribs of geogrids.

At present, the pullout tests usually measure the pullout force and displacement and then the relationship between the normal stress and the relative displacement by calculation, but the progressive yield mechanism of interface is not considered. Baker et al. [21] studied the progressive mechanism of interfacial friction in the pullout test. Nakamura et al.'s research results [22] show that there is deformation of reinforcement in the drawing test, and the interface friction resistance gradually develops. Ma et al. [23] divided the exertion of interfacial friction resistance in the pullout test into initial stage, local yield stage, and complete yield stage. Current research result shows that there are less theoretical studies on the interaction mechanism between reinforcement and soil. Gurung et al. [24] studied the 1-D expression of shear stress and displacement that was capable to analyze small strain cases. Filz et al. [25] drew the softening curve of shear stress shear displacement and obtained the plastic displacement softening model and plastic work softening model by hyperbolic fitting. Zhu et al. and Zhang et al. [26, 27] used a three-parameter model to simulate the progressive failure characteristics of fibers at the interface of fiber reinforced soil. Li et al. [28] obtained the analytical solutions of the pullout force, displacement, and shear stress of the reinforcement material without considering the softening characteristics of the reinforced soil interface. Cheng et al. [29] studied the shear behavior of geogrid-soil interface and its statistical damage softening model.

In this paper, the pullout characteristics of the interface between sand and geogrid are studied by the large-scale indoor pullout test. On this basis, the damage theory is introduced to establish the damage softening model which can describe the softening characteristics of geogrid-soil interface. The pullout process of strain-softening reinforcement is divided into elastic stage, softening-elastic stage, pure softening stage, residual-softening stage, and residual stage. Based on the basic control equation and damage theory of geogrid-soil interface, the expressions of interface tension, shear stress, and displacement at different stages of reinforcement of strain softening, under pullout load, are derived, respectively, which reflect the progressive failure of the pullout interface between reinforcement and soil. Finally, the proposed model is verified by the test results. The research results provide technical reference for reasonable selection of reinforcement materials in reinforced soil engineering.

2. Pullout Test of Geogrid

2.1. Test Materials. The reinforcement material is unidirectional tensile HDPE plastic geogrid, and width and thickness of the geogrid sample are 30 cm and 6 mm, respectively, as shown in Figure 1. The spacing between transverse ribs of geogrid used in this test is 35 cm and 50 cm, respectively. The technical indexes of geogrid are shown in Table 1. The physical and mechanical indexes of sand selected for filling are obtained through the particle screening test, relative density test, and direct shear test, as shown in Table 2. Coarse sand with good grading is used for filling, and the grain grading curve is shown in Figure 2.

2.2. Test Scheme. The pullout equipment was mainly composed of four parts: pullout box, normal loading system, horizontal loading system, and data acquisition system. The pullout box was made of 10 mm thick steel plate and was 600 mm in length, 400 mm in width, and 500 mm in height in internal dimensions, as shown in Figure 3. The test filling height is 50 cm, which is compacted in four layers, and compaction degree is taken as 90%. The normal stresses, 50 kPa, 100 kPa, 150 kPa, and 200 kPa, are applied to the test chamber filled with coarse sand. According to the Test Methods of Geosynthetics for Highway Engineering (JTG E50-2006) [30] and considering the large mesh size of geogrid, the pullout rate during the test is 1 mm/min, so as to ensure that the geogrid will not produce torsion during the test. When the pullout force is no longer increased or continues to decrease, stop the test. In the test, lubricant was applied on the inner surface of the four walls of the box to reduce the friction between the box wall and the soil. The width of the sample was controlled to ensure a certain distance between the geogrid and the side wall of the box, so as to minimize the influence of boundary effect and size effect.

2.3. Test Results. The relationship curve of pullout force and displacement with different transverse rib spacing under different normal stress is shown in Figure 4. It can be seen that with the increase of pullout displacement, pullout curve shows strain-softening trend after reaching the peak value. In the softening process, with the continuous increase of pullout displacement, pullout force gradually tends to a stable value, that is to say, the residual strength value. The larger the normal stress, the larger the displacement corresponding to the maximum drawing force.

The reason is that the interface progressive yield mechanism gradually plays a role with the increase of pullout displacement. With the increase of normal stress, the

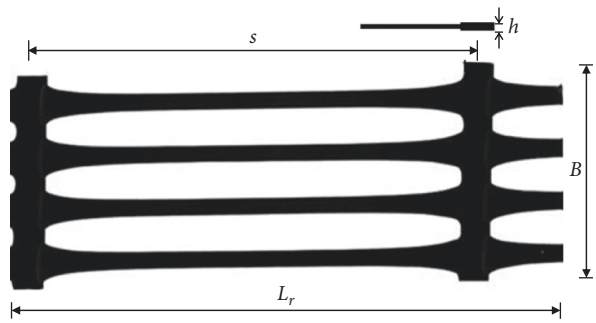

Figure 1: Uniaxial geogrids.

Table 1: The technical indexes of geogrid.

Transverse rib spacing (cm)	Tensile strength (kN/m)	Tensile strength at 2% strain (kN/m)	Tensile strength at 5% strain (kN/m)	Peak strain (%)
35	183.2	66.76	136.91	7.24
50	175.0	58.63	109.86	8.93

Table 2: The physical and mechanical indexes of soil.

Specific gravity	Experimental relationship (g/cm^3)	Maximum dry density (g/cm^3)	Void ratio	Nonuniform coefficient (C_u)	Curvature coefficient (C_c)	Cohesion (kPa)	Internal friction angle (°)
2.65	1.42	1.83	0.74	5.31	1.42	1	26.5

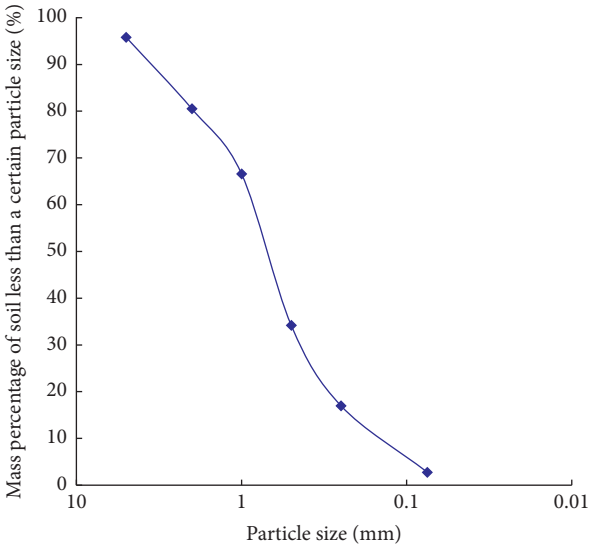

Figure 2: The soil grading curve.

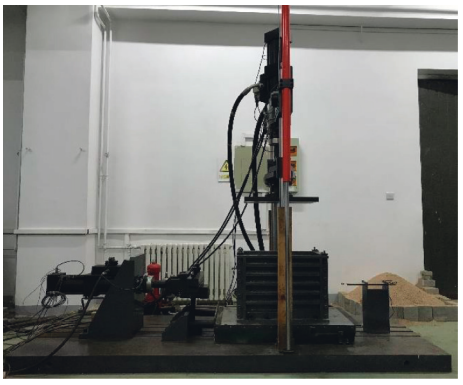

Figure 3: The pullout test equipment.

stronger the restraint effect of geogrid-soil interface is, the slower the progressive exertion process of geogrid-soil interface load is, and more displacement is required when the pullout force reaches the peak value.

According to the Mohr–Coulomb strength criterion, the maximum shear stress and normal stress of geogrid-soil interface are fitted, as shown in Figure 5. It can be seen that the maximum shear stress at the interface increases linearly with the increase of normal stress. The parameters of peak shear strength at the geogrid-soil interface are obtained from the fitting results, as shown in Table 3. For the transverse rib spacing of 35 cm, the cohesion and friction angle of geogrid-soil interface are 13.55 kPa and 4.23°, respectively. For the transverse rib spacing of 50 cm, the cohesion and friction angle of geogrid-soil interface are 10.35 kPa and 4.11°, respectively. However, cohesion and friction angle of pure sand are 1 kPa and 26.5°, respectively. The reinforcement of geogrid improves the cohesion of soil, but the friction angle decreases.

3. Mechanical Analysis of Geogrid-Soil Interface

During the pullout test, the geogrid is placed in the middle of the upper and lower test chambers. The top of the upper box is applied with vertical compressive stress, and geogrid is pulled out slowly. The schematic diagram of the pullout

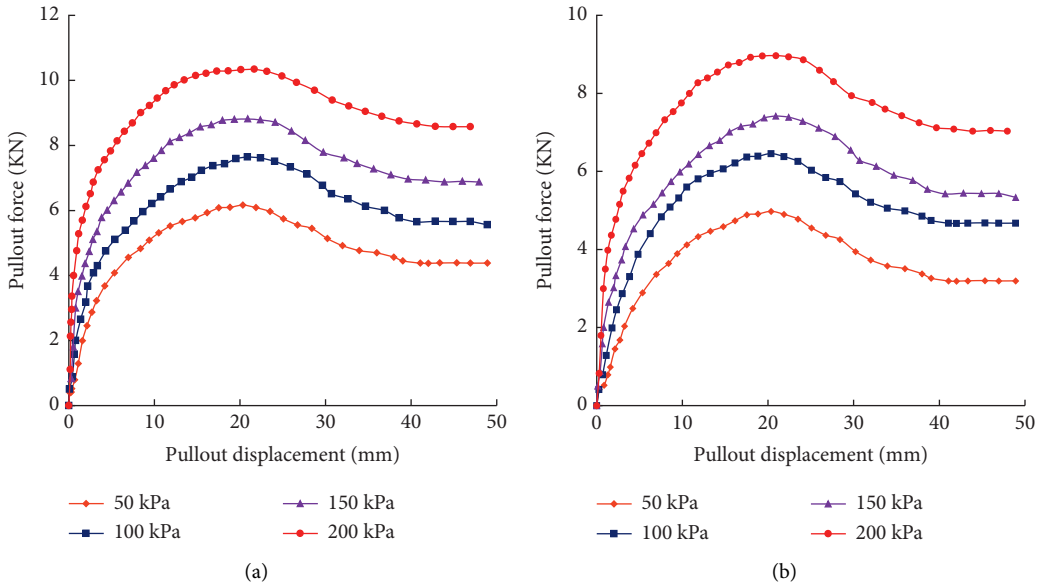

Figure 4: The curve between pullout displacement and force of different transverse rib spacings. (a) $s = 35$ cm. (b) $s = 50$ cm.

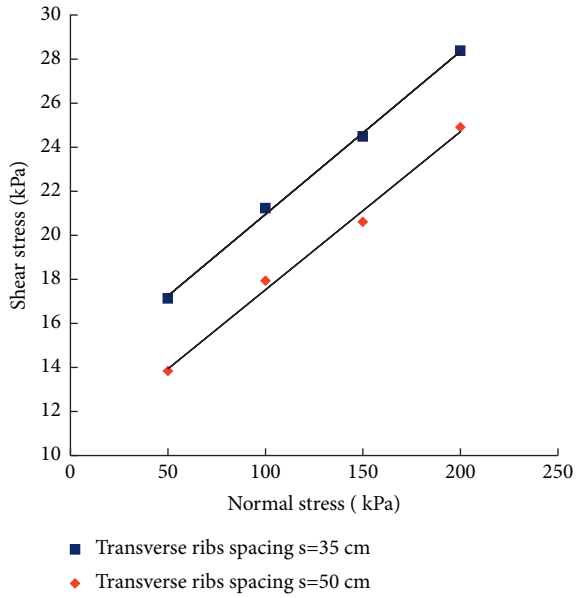

Figure 5: Relationship between interfacial shear strength and normal stress.

Table 3: Strength parameters of geogrid-soil interface.

Transverse rib spacing s (cm)	Cohesion c (kPa)	Friction angle φ (°)
35	13.55	4.23
50	10.35	4.11

process is shown in Figure 6. Geogrid is assumed to be an axially loaded tension member; when a pullout force F is applied, shear stresses are mobilized at the geogrid-soil interface to resist the pullout force. The microelement with length of x is taken along the length direction of geogrid; according to the force balance and physical and geometric equations,

$$dF(x) + 2\tau(x)dx = 0, \tag{1}$$

$$F(x) = E_r\varepsilon(x) = -E_r\frac{du(x)}{dx}, \tag{2}$$

where x = arbitrary coordinate as shown in Figure 6; $F(x)$ = pullout force at point x; $u(x)$ = displacement at point x; $\varepsilon(x)$ = tensile strain at point x; $\tau(x)$ = interface shear stress at an arbitrary point x; E_r = tensile stiffness, $E_r = Et$; E is elastic modulus of geogrid; and t is thickness of geogrid.

According to (1) and (2), the basic equation of load transfer can be expressed as

$$E_r\frac{d^2u(x)}{dx^2} - 2\tau(x)dx = 0. \tag{3}$$

In the pullout test of geogrid, the pullout force F at pulling end can be measured by the sensor, and the force at free end can be ignored. The boundary condition of the pullout force at both ends of the geogrid can be expressed as

$$F(0) = -E_r\frac{du(x)}{dx}\Big|_{x=0} = F,$$
$$F(l) = -E_r\frac{du(x)}{dx}\Big|_{x=l} = 0. \tag{4}$$

In the process of pullout, it is necessary to establish the constitutive model of the geogrid-soil interface to solve $u(x)$ and $\tau(x)$ in (3).

4. Damage Softening Model of Geogrid-Soil Interface under Pullout Load

A trilinear softening model is adopted to quantify the shear stress-displacement relationship of the geogrid-soil interface, as depicted in Figure 7. In this model, the geogrid-soil interface first behaves elastically, which is characterized by

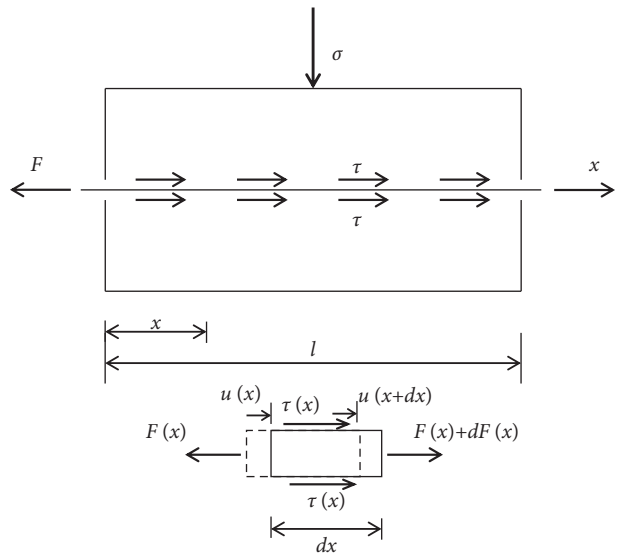

Figure 6: Schematic illustration of pullout mechanism of geogrid in soil.

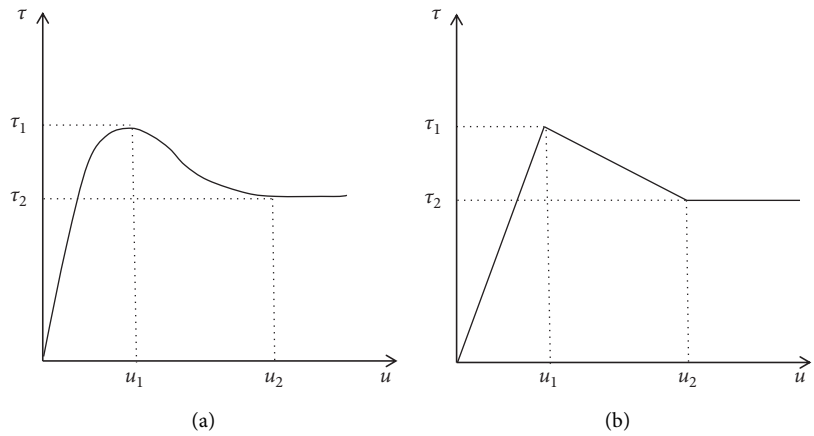

Figure 7: Strain-softening model of geogrid-soil interface. (a) Curve relationship of shear stress-displacement. (b) Trilinear softening model.

an ascending branch up to the peak shear resistance. Afterward, stress softening emerges at the of geogrid-soil interface. Once the interfacial shear stress decreases to the residual shear resistance, the shear stress remains constant.

In order to consider the strain-softening constitutive model of geogrid-soil interface with damage, according to Rabotnov damage factor D, the geogrid-soil interface under pullout force is assumed to be composed of damaged and undamaged parts, as shown in Figure 7. The damage factor D can be expressed as the ratio of the damage length to the original length, which can be expressed as

$$D = \frac{d''(x)}{d(x)}, \tag{5}$$

$$\tau(x)d(x) = \tau'(x)d'(x) + \tau''(x)d''(x), \tag{6}$$

where $d(x)$ = initial original length of geogrid-soil interface; $d'(x)$ = undamaged part length; $d''(x)$ = damaged part length; $\tau(x)$ = apparent shearing stress at point x; $\tau'(x)$ = shear stress of undamaged length; and $\tau''(x)$ = shear stress of damaged length.

According to (5) and (6), expression can be expressed as

$$\tau(x) = \tau'(x)(1 - D) + \tau''(x)D. \tag{7}$$

It can be seen from formula (7) that the damage factor variable D represents the damage degree of the geogrid-soil interface in the process of pullout, and the damage factor D satisfies $0 \le D \le 1$.

It can be seen from Figure 8 that the shear strength of geogrid-soil interface reaches the peak shear stress τ_1; afterward, the strength decreases until it reaches the stable residual strength τ_2. In the damage model, the shear stress of damaged length is not zero and still bear the shear stress of τ_2, that is $\tau'' = \tau_2$; formula (7) can be expressed as

$$\tau = \tau'(1 - D) + \tau_2 D. \tag{8}$$

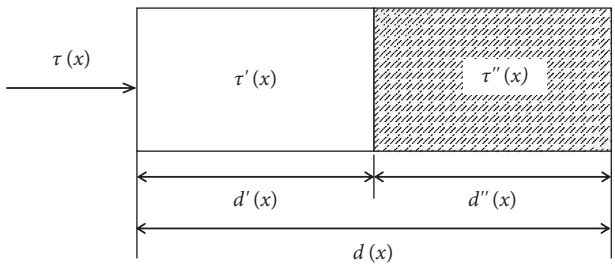

Figure 8: Micro-stress analysis of geogrid-soil interface.

For the undamaged part, the shear stress $\tau'(x)$ still obeys the linear part of the initial interface shear stress-displacement, and formula (8) can be expressed as

$$\tau = Gu(1 - D) + \tau_2 D. \tag{9}$$

According to Lemaitre's strain equivalent principle [31], the constitutive relation of damage state is the same as undamaged state. Under the effect of damage, the relationship of shear stress-displacement is obtained by multiplying the damage factor variable D. For $0 \le u \le u_1$, the effect of damage is ignored; for $u_1 \le u \le u_2$, the damage factor variable satisfies $0 < D < 1$; for $u \ge u_2$, the damage factor variable satisfies $D = 1$.

For trilinear shear stress-displacement softening model, relationship between shear stress $\tau(x)$ and shear displacement $u(x)$ can be expressed by

$$\tau(x) = \begin{cases} Gu, & 0 \le u < u_1, \quad (a), \\ D\left[2\tau_1 - Gu(x)\right], & u_1 \le u \le u_2, \quad (b), \\ \tau_2, & u \ge u_2, \quad (c), \end{cases} \tag{10}$$

where G = shear stiffness at the geogrid-soil interface that should be determined experimentally and u_1 and u_2 = shear displacement corresponding to the peak shear resistance τ_1 and the residual shear resistance τ_2, respectively. Considering that $u_1 = \tau_1/G$ and $u_2 = (2\tau_1\text{-}\tau_2)/G$, in order to simplify the calculation, it is assumed that the slopes of the ascending and descending sections in the interface softening model are equal, and both of them are taken as G.

Based on the above assumptions, the progressive pullout behavior of geogrid in soil can be divided into five consecutive phases, as shown in Figure 9. These five phases are described as follows: (I) initial pure elastic phase—the relationship between shear stress and displacement is linear; (II) softening-elastic phase—a transition point P_1, as shown in Figure 9(b), is introduced here to divide the elastic and softening zones; (III) pure softening phase; (IV) softening-residual phase—similar to Phase II, once the interfacial shear stress at the pullout end decreases to the residual shear resistance, the geogrid turns into the softening-residual transition state; again, a transition point P_2 is introduced here to divide the softening and residual zones, as shown in Figure 9(d); in this phase, both the pullout force and the interfacial shear stress decrease slightly; (V) final pure residual phase—the final stage starts when the interfacial shear stress at the free end decreases to the residual shear resistance. As shown in Figure 9(e), the residual zone now occupies the entire geogrid. In this stage, the pullout force remains constant, whereas the pullout displacement increases continuously.

5. The Pullout Process of Damage Softening Process

5.1. Elastic Stage. In this phase, the relationship between the interfacial shear stress and the shear displacement can be expressed by (10). By combining (3) and (10), we get

$$\frac{\mathrm{d}^2 u_e(x)}{\mathrm{d}x^2} - \alpha^2 u_e(x) = 0, \tag{11}$$

where $\alpha = \sqrt{2G/E_r}$ and α is the interface influence coefficient which reflects the influence of geogrid on the tensile force distribution.

A general solution of (11) is

$$u_e(x) = C_1 e^{\alpha x} + C_2 e^{-\alpha x}, \tag{12}$$

where C_1 and C_2 = integration constants, which can be determined with specific boundary conditions.

The solution of the boundary-value problem defined by (4) and (12) is

$$u_e(x) = \frac{F}{E_r \cdot \alpha} \frac{\cosh[\alpha(l - x)]}{\sinh(\alpha l)}. \tag{13}$$

The corresponding interfacial shear stress $\tau_e(x)$ and pullout force $F_e(x)$ are then calculated using (10) and (2), respectively, which can be expressed by

$$\begin{aligned} \tau_e(x) &= \frac{GF}{E_r \alpha} \frac{\cosh[\alpha(l - x)]}{\sinh(\alpha l)}, \\ F_e(x) &= \frac{F}{\alpha} \frac{sinh[\alpha(l - x)]}{\sinh(\alpha l)}. \end{aligned} \tag{14}$$

5.2. Softening-Elastic Stage. When the pullout force continues to increase, the pulling end begins to soften, that is, the geogrid within the range of (0~ l_s) from the pulling end enters the softening stage, while the geogrid within ($l_s \sim l$) is still in elastic state, as shown in Figure 9(b).

In the elastic zone, the distributions of tensile force, interfacial shear stress, and shear displacement in the elastic zone ($l_s \sim l$) are similar to those in the pure elastic phase. Therefore, the following equations are easily obtained:

$$\begin{aligned} u_e(x) &= \frac{F'}{E_r \cdot \alpha} \frac{\cosh\left[\alpha(l - l_s - x)\right]}{\sinh\left[\alpha(l - l_s)\right]}, \\ \tau_e(x) &= \frac{GF'}{E_r \alpha} \frac{\cosh\left[\alpha(l - l_s - x)\right]}{\sinh\left[\alpha(l - l_s)\right]}, \\ F_e(x) &= \frac{F'}{\alpha} \frac{sinh\left[\alpha(l - l_s - x)\right]}{\sinh\left[\alpha(l - l_s)\right]}, \end{aligned} \tag{15}$$

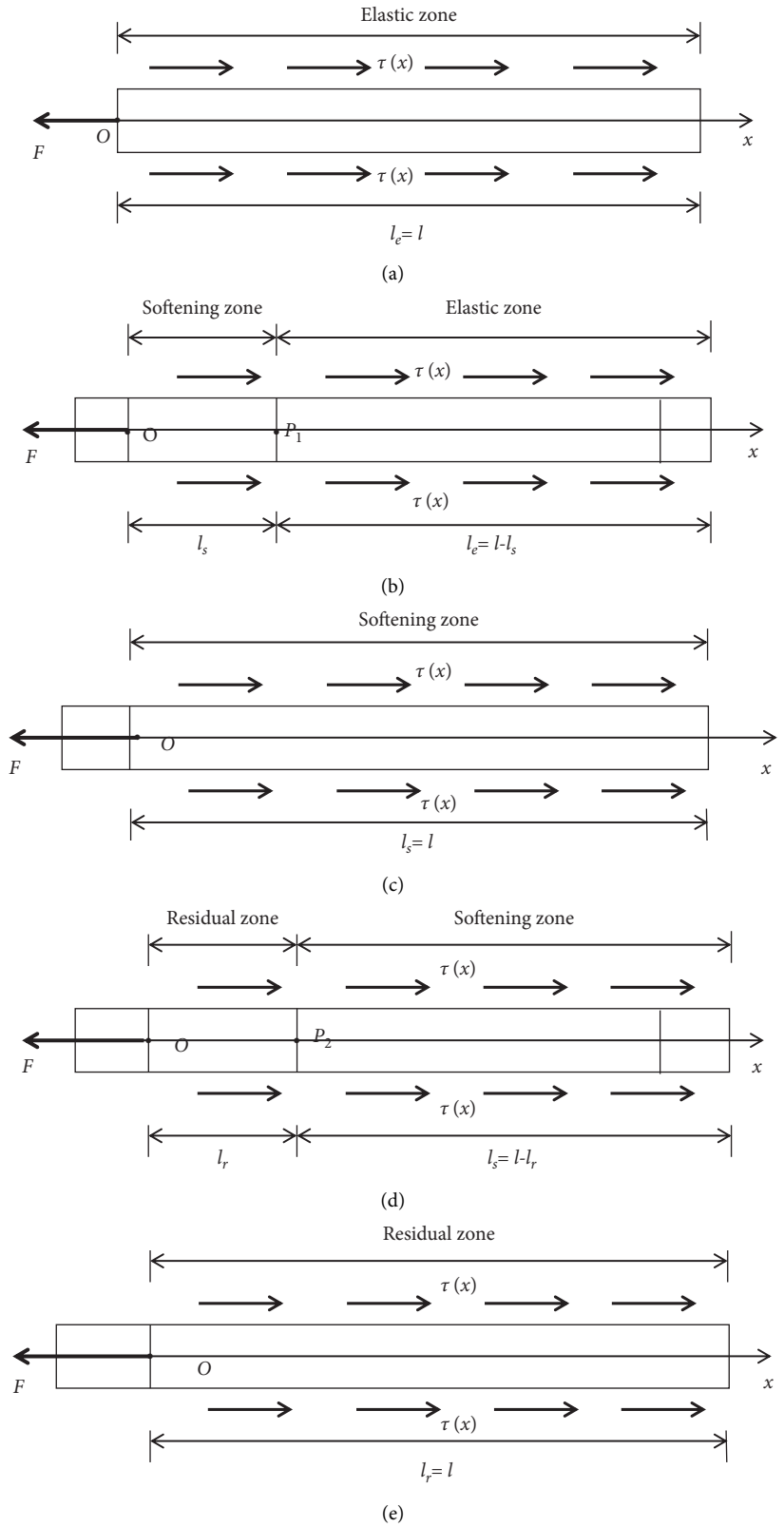

Figure 9: Progressive pullout process of geogrid in softening model. (a) Elastic phase. (b) Softening-elastic phase. (c) Softening phase. (d) Residual-softening phase. (e) Residual phase.

where l_{hs} = length of the softening zone and F' = tensile force at the transition point P. Considering that the interfacial shear stress at P equals the peak shear resistance, we get

$$F' = \frac{E_r \alpha \tau_1}{G} \frac{\cosh[\alpha(l-2l_s)]}{\sinh[\alpha(l-l_s)]}. \tag{16}$$

In the softening zone (0~l_s), the relationship between the interfacial shear stress and the shear displacement is defined by (10). Combining (3) and (10), we get

$$\frac{d^2 u_s(x)}{dx^2} + \beta^2 u_s(x) = \frac{4\ D\tau_1}{E_r}. \tag{17}$$

A general solution of (17) is

$$u_s(x) = C_3 \cos(\beta x) + C_4 \sin(\beta x) + \frac{4\ D\tau_1}{E_r}. \tag{18}$$

Accordingly, the solutions for the softening zone are

$$\begin{aligned}
u_s(x) &= \left\{ \frac{\tau_1 \sin n[2\beta(l-l_s)]}{2G \sin(\beta l_s) \cdot \sinh^2[\beta(l-l_s)]} - \frac{F}{E_r \beta} \cot \beta l_s \right\} \cdot \cos \beta x - \frac{F}{E_r \beta} \sin \beta x + \frac{4\ D\tau_1}{E_r}, \\
F_s(x) &= \left\{ \frac{\tau_1 \beta E_r \sin n[2\beta(l-l_s)]}{2G \sin(\beta l_s) \cdot \sinh^2[\beta(l-l_s)]} - F \cot \beta l_s \right\} \cdot \sin \beta x + F \cos \beta x, \\
\tau_s(x) &= 2\ D\tau_1 - \left\{ \frac{D\tau_1 \sin n[2\beta(l-l_s)]}{2G \sin(\beta l_s) \cdot \sinh^2[\beta(l-l_s)]} - \frac{DF}{E_r \beta} \cot \beta l_s \right\} \cdot \cos \beta x + \frac{DF}{E_r \beta} \sin \beta x - \frac{4\ D\tau_1}{E_r}.
\end{aligned} \tag{19}$$

5.3. Softening Stage. Similar to the analysis of the softening zone in the softening-elastic phase, (17) is still applicable in the pure softening phase. The boundary conditions are

$$\begin{aligned}
F_s(x)|_{x=0} &= F, \\
F_s(x)|_{x=l} &= 0.
\end{aligned} \tag{20}$$

The solutions for the pure softening phase are

$$F_s(x) = \frac{F \cot \alpha l}{\alpha} \sin \beta x + \frac{F}{E_r} \cos \beta x, \tag{21}$$

$$u_s(x) = \frac{F \cot \beta l}{E_r \beta^2} \cos \beta x - \frac{F}{E_r \beta} \sin \beta x + \frac{4\ D\tau_1}{E_r}, \tag{22}$$

$$\tau_s(x) = 2\ D\tau_1 - \frac{G \cdot D \cdot F \cot \beta l}{E_r \beta^2} \cos \alpha x + \frac{G \cdot D \cdot F}{E_r \beta} \sin \beta x - \frac{4G \cdot D \cdot \tau_1}{E_r}. \tag{23}$$

5.4. Residual-Softening Stage. As the pullout force decreases, the residual state initiates at the pulling end and extends towards the free end. The residual and softening zones are divided by the transition point P_2. In the softening zone, the distributions of tensile force, interfacial shear stress, and shear displacement are given by (22)–(24), respectively, with x replaced by (x-l_r), l by (l -l_r), and F by F'.

$$F_s(x) = \frac{F' \cot \beta(l-l_r)}{\beta} \sin \beta(x-l_r) + \frac{F'}{E_r} \cos \beta(x-l_r), \tag{24}$$

$$u_s(x) = \frac{F' \cot \beta(l-l_r)}{E_r \beta^2} \cos \beta(x-l_r) - \frac{F'}{E_r \beta} \sin \beta(x-l_r) + \frac{4\ D\tau_1}{E_r}, \tag{25}$$

$$\tau_s(x) = 2\ D\tau_1 - \frac{G \cdot D \cdot F' \cot \beta(l-l_r)}{E_r \beta^2} \cos \beta(x-l_r) + \frac{G \cdot D \cdot F'}{E_r \beta} \sin \beta(x-l_r) - \frac{4G \cdot D \cdot \tau_1}{E_r}. \tag{26}$$

Because the interfacial shear stress at P_2 equals the residual shear resistance, F' in equations (25)–(27) can be rewritten as

$$F\prime = \left[\frac{E_r\beta^2}{G}\left(2\tau_1 - \frac{\tau_2}{D}\right) - 4\tau_1\beta^2\right]\tan\beta l. \tag{27}$$

As for the residual zone, the interfacial shear stress is equal to the residual shear resistance. (1) leads to

$$dF_r(x) = -2\tau_2 dx\ . \tag{28}$$

Combining it with the boundary conditions,

$$\begin{aligned} F_r(x)|_{x=0} &= F, \\ F_r(x)|_{x=l_r} &= F_s(x)|_{x=l_r}. \end{aligned} \tag{29}$$

The distribution of tensile force is obtained by integrating (28):

$$F_r(x) = -2\tau_2 x + \left[\frac{\beta^2}{G}\left(2\tau_1 - \frac{\tau_2}{D}\right) - \frac{4\tau_1\beta^2}{E_r}\right]\tan\beta l + 2\tau_2 l_r. \tag{30}$$

Substituting (30) into (2) and considering P_2,

$$u_r(x)|_{x=l_r} = u_s(x)|_{x=l_r}. \tag{31}$$

The shear displacement in the residual zone can be expressed by

$$u_r(x) = -\frac{\tau_2 x^2}{E_r} - \left\{\left[\frac{\beta^2}{G}\left(2\tau_1 - \frac{\tau_2}{D}\right) - \frac{4\tau_1\beta^2}{E_r}\right]\tan\beta l + 2\tau_2 l_r\right\}x + C_5, \tag{32}$$

where C_5 = the constant term which can be obtained according to (31).

5.5. Residual Stage. In residual stage, the pullout force of geogrid does not change any more. The interfacial shear stress of the whole area of geogrid is τ_2, and the pullout force of geogrid is linear distribution:

$$F_r(x) = -2\tau_2(l - x). \tag{33}$$

Pullout displacement of geogrid at this stage is u_r^0; therefore, the distribution of tensile force is given as

$$F_r(x) = \frac{\tau_2(l - x)^2}{E_r} + u_r^0. \tag{34}$$

6. Determination of Model Parameters

In the trilinear shear stress-displacement damage softening model of geogrid-soil interface, α and β are the interface pullout influence coefficients, $\alpha = \sqrt{2G/E_r}$, and $\beta = \sqrt{2\ DG/E_r}$, where G = the shear stiffness of geogrid-soil interface (it represents the slope of the straight line in the shear stress-displacement curve); E_r is the tensile modulus of geogrid, $E_r = Et$, where E is the elastic modulus and t is the thickness of geogrid; and D is the damage factor variable; assuming that it is a function of interface displacement, the damage evolution law of geogrid-soil interface is expressed by two-parameter Weibull distribution function [29, 32], that is,

$$D = 1 - \exp\left[-\left(\frac{u}{u_0}\right)^m\right], \tag{35}$$

where m = the shape parameter of Weibull function, which reflects the shape of the function, and u_0 = the scale parameter of Weibull function, which can enlarge and reduce the abscissa scale of curve, but does not affect the shape of curve, and it is a parameter related to the average value of all parameters.

Combining (9) and (35), the interface shear stress of the model is

$$\tau = Gu\ \exp\left[-\left(\frac{u}{u_0}\right)^m\right] + \tau_2\left\{1 - \exp\left[-\left(\frac{u}{u_0}\right)^m\right]\right\}. \tag{36}$$

The parameters u_0 and m are determined, according to the characteristics of the τ-u curve of geogrid-soil interface. It can be seen from Figure 7 that the τ-u curve has obvious characteristics of strain softening, with peak value and residual. When the displacement reaches u_1 and the stress reaches the peak point, the stress increment at this point is zero, which can be expressed as

$$\frac{\partial\tau}{\partial u}|_{u=u_1} = 0, \tag{37}$$

$$\tau_1 = Gu_1\ \exp\left[-\left(\frac{u_1}{u_0}\right)^m\right] + \tau_2\left\{1 - \exp\left[-\left(\frac{u_1}{u_0}\right)^m\right]\right\}, \tag{38}$$

where τ_1 is peak shear stress at geogrid-soil interface and u_1 is the interface displacement corresponding to τ_1. Combining (37) and (38), the parameters m and u_0 are

$$\begin{aligned} m &= \frac{Gu_1}{(Gu_1 - \tau_2)\left[\ln\left(\tau_1 - \tau_2/Gu_1 - \tau_2\right)\right]}, \\ u_0 &= \left[\frac{m(Gu_1 - \tau_2)u_1^{m-1}}{G}\right]^{1/m}. \end{aligned} \tag{39}$$

7. Verification of Interface Constitutive Model

According to the pullout test results of geogrids with different transverse rib spacings, the parameters of the trilinear shear stress-displacement damage softening model of the geogrid-soil interface are obtained, as shown in Table 4. It can be seen that the shear stiffness G decreases with the increase of transverse rib spacing, but increases with the increase of normal stress. In Weibull distribution, parameters u_0 and m basically do not change the basic shape of the model curve, but with the increase of parameters u_0 and m, the curve moves upward, that is, the peak value of interfacial shear stress and residual shear stress increases.

By substituting the model parameters into the expressions of drawing force, displacement, and interfacial shear stress at different drawing stages, the theoretical calculation results of the trilinear shear stress-displacement damage softening model are obtained, as shown in Figure 10. It can be seen that the calculated results of the model are in good

Table 4: Model parameters of geogrid-soil interface.

s (cm)	σ (kPa)	E_r (kN·m^{-1})	G (kPa·mm^{-1})	u_0 (mm)	m
35	50	0.56×10^3	4.23	1.063	2.954
	100	0.56×10^3	5.56	1.184	3.519
	150	0.56×10^3	6.45	1.395	4.614
	200	0.56×10^3	8.25	1.512	5.485
50	50	0.45×10^3	2.36	1.006	2.329
	100	0.45×10^3	3.35	1.054	2.953
	150	0.45×10^3	4.76	1.147	3.258
	200	0.45×10^3	5.73	1.324	4.124

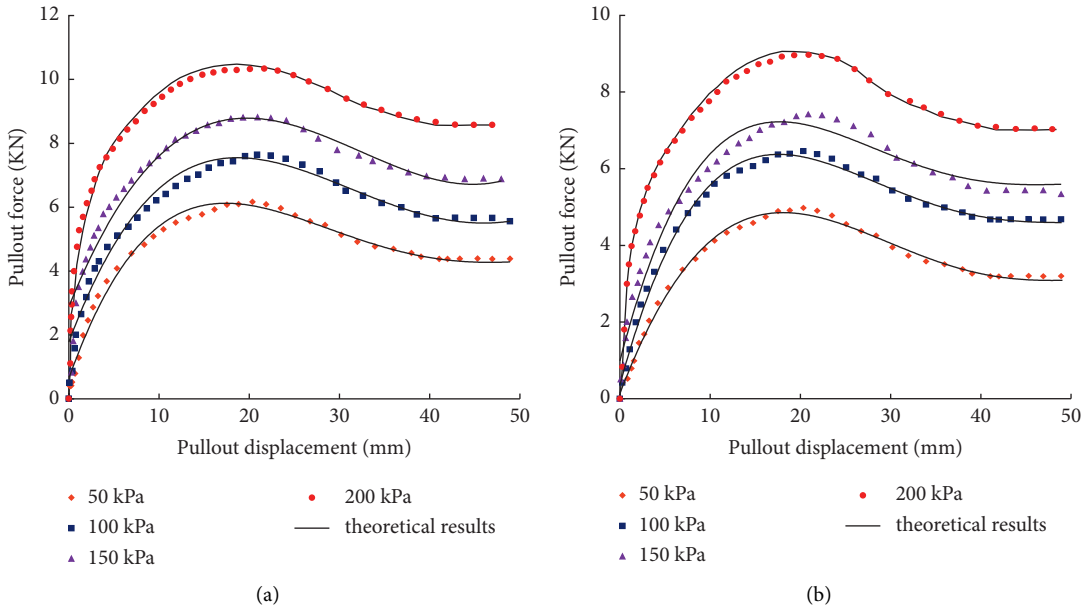

Figure 10: Comparison of test results and theoretical results. (a) $s = 35$ cm. (b) $s = 50$ cm.

agreement with the laboratory test curves, which can correctly reflect the strain-hardening characteristics of the geogrid-soil interface and the strain damage softening characteristics considering the damage effects during the pullout process, better reflect the trilinear damage softening model, and can accurately analyze the interaction mechanism of geogrid-soil interface.

8. Conclusions

The main conclusions of the present work can be summarized as follows:

(1) In the pullout test, the strain-softening phenomenon appears after the pullout force and displacement curve reach the peak value. The shear strength of the geogrid-soil interface increases with the increase of normal stress, which shows that the reinforcement of geogrid can improve the cohesion of soil, but the internal friction angle decreases. Based on the damage mechanics, the damage softening model is established to describe the softening characteristics of geogrid-soil interface. The mechanism of geogrid-soil interface considering damage is revealed theoretically.

(2) In order to analyze the strain-softening behaviors of geogrid-soil interface, the trilinear shear stress-displacement damage softening model is used to describe the interaction mechanism of the geogrid-soil interface. Based on the damage softening model, the whole pullout process is divided into five stages, namely, pure elastic stage, softening-elastic stage, softening stage, residual-softening stage, and residual stage.

(3) The analytical solutions of interface tension, shear stress, and displacement at different stages of damage softening characteristics under the pullout load are derived through the basic interface control equation. Meanwhile, the evolution law of interface shear stress in different pullout stages is analyzed, which reflects the progressive failure of geogrid-soil interface.

(4) Considering the influence of residual strength, the damage softening constitutive model can analyze the whole pullout process of geogrid-soil interface. Compared with pullout results, prediction results of the model are basically consistent with the pullout test, which verifies the effectiveness and rationality of model for progressive failure analysis in the pullout interface.

Data Availability

The data used to support the findings of this study are available from the corresponding author upon request.

Conflicts of Interest

The authors declare that they have no conflicts of interest.

Acknowledgments

The study was supported by Hebei Province Natural Science Foundation (grant nos. E2019208159 and E2020208071), Hebei Key Laboratory of Geotechnical Engineering Safety and Deformation Control (grant no. HWEKF202102), State Key Laboratory of Mechanical Behavior and System Safety of Traffic Engineering Structures (grant no. 1902), Doctoral Research Startup Fund of Hebei University of Science and Technology (grant no. 1181482), and The Project of Talent Introduction of Hebei Province in 2021 (Key Technologies of Intelligent Construction of New Engineering).

References

[1] C. G. Bao, M. Y. Wang, and J. H. Ding, "Mechanism of soil reinforced with geogrid," *Journal of Yangtze River Scientific Research Institute*, vol. 30, no. 1, pp. 34–41, 2013.

[2] K. Sweta and S. K. K. Hussaini, "Effect of shearing rate on the behavior of geogrid-reinforced railroad ballast under direct shear conditions," *Geotextiles and Geomembranes*, vol. 46, no. 3, pp. 251–256, 2018.

[3] F. Y. Liu, H. L. Hu, and J. Wang, "Influence of cyclic shear behavior of geogrid-soil interface," *China Journal of Highway and Transport*, vol. 32, no. 12, pp. 115–122, 2019.

[4] K. F. Liu, J. P. Xu, and Q. S. Zhou, "Large-scale direct shear tests on properties of geogrid-soil interfaces," *Chinese Journal of Geotechnical Engineering*, no. A01, pp. 185–188, 2019.

[5] J. Q. Wang, Y. F. Zhou, and X. Y. Tang, "Development and application of large size direct shear test apparatus with visual and digital collection functions for reinforced soil," *Rock and Soil Mechanics*, vol. 38, no. 5, pp. 1533–1540, 2017.

[6] F. C. Liu, M. T. Wu, and J. Yang, "Experimental study of strength characteristics of geogrid reinforced rubber sand mixtures," *Rock and Soil Mechanics*, vol. 4, no. 2, pp. 580–591, 2019.

[7] X. F. Zhou, M. X. Zhang, and C. C. Qiu, "Strength of sand reinforced with different forms of geogrid," *Journal of Shanghai Jiao Tong University*, vol. 47, no. 9, pp. 1377–1381, 2013.

[8] Z. J. Wang, F. Jacobs, and M. Ziegler, "Influence of geogrid transverse members on strength and deformation behavior of reinforced granular soil," *Rock and Soil Mechanics*, vol. 38, no. 8, pp. 2234–2240, 2017.

[9] Y. Kang, B. Nam, J. G. Zornberg, and Y.-H. Cho, "Pullout resistance of geogrid reinforcement with in-plane drainage capacity in cohesive soil," *KSCE Journal of Civil Engineering*, vol. 19, no. 3, pp. 602–610, 2015.

[10] G. Q. Yang, G. X. Li, and B. J. Zhang, "Experimental studies on interface friction characteristics of geogrids," *Chinese Journal of Geotechnical Engineering*, vol. 28, no. 8, pp. 948–952, 2006.

[11] M. Y. Wang, C. G. Bao, and J. H. Ding, "Effect of some test conditions on pullout behaviors of interface between geogrids and compacted expansive soils," *Rock and Soil Mechanics*, vol. 29, no. s1, pp. 81–84, 2008.

[12] C. Z. Xiao and X. J. Feng, "Pullout-test analysis on properties of interface between geogrid ang clay," *Journal of Civil, Architectural & Environmental Engineering*, vol. 34, no. 3, pp. 47–51, 2012.

[13] W. Z. Cao, J. J. Zheng, and Y. J. Zhou, "Experimental investigation of deformation and geogrid-soil interface behavior of triaxial geogrid," *Journal of Southwest Jiaotong University*, vol. 51, no. 5, pp. 840–846, 2016.

[14] J. J. Zheng, W. Z. Cao, and Y. J. Zhou, "Pullout test study of interface behavior between triaxial geogrid and soil," *Rock and Soil Mechanics*, vol. 38, no. 2, pp. 317–324, 2017.

[15] J. Jin, G. Q. Yang, and W. C. Liu, "Experimental study of effects of transverse ribs spacing on pullout characteristics of geogrids," vol. 38, no. 2, pp. 317–324, 2017.

[16] M. R. Abdi and A. R. Zandieh, "Experimental and numerical analysis of large scale pull out tests conducted on clays reinforced with geogrids encapsulated with coarse material," *Geotextiles and Geomembranes*, vol. 42, no. 5, pp. 494–504, 2014.

[17] Z. Wang, F. Jacobs, and M. Ziegler, "Experimental and DEM investigation of geogrid-soil interaction under pullout loads," *Geotextiles and Geomembranes*, vol. 44, no. 3, pp. 230–246, 2016.

[18] A. M. N. Alagiyawanna, M. Sugimoto, S. Sato, and H. Toyota, "Influence of longitudinal and transverse members on geogrid pullout behavior during deformation," *Geotextiles and Geomembranes*, vol. 19, no. 8, pp. 483–507, 2001.

[19] N. Moraci and P. Recalcati, "Factors affecting the pullout behaviour of extruded geogrids embedded in a compacted granular soil," *Geotextiles and Geomembranes*, vol. 24, no. 4, pp. 220–242, 2006.

[20] G. Cardile, D. Gioffrè, N. Moraci, and L. S. Calvarano, "Modelling interference between the geogrid bearing members under pullout loading conditions," *Geotextiles and Geomembranes*, vol. 45, no. 3, pp. 169–177, 2017.

[21] R. M. Bakeer, S. M. Sayed, P. Cates, and R. Subramanian, "Pullout and shear tests on geogrid reinforced lightweight aggregate," *Geotextiles and Geomembranes*, vol. 16, no. 2, pp. 119–133, 1998.

[22] T. Nakmura, T. Mitachi, and I. Ikeura, "Estimating method for the in-soils deformation behavior of geogrid based on the results of derect box shear test," *Journal of the Japanese Geotechnical Society Soils and Foundation*, vol. 43, no. 1, pp. 47–57, 2003.

[23] C. M. Ma, Y. T. Zhou, and H. L. Liao, "Experimental study on interface friction of plastic geogrid reinforced earth," *China Railway Science*, vol. 25, no. 3, pp. 36–39, 2005.

[24] N. Gurung, "1-D analytical solution for extensible and inextensible soil/rock reinforcement in pull-out tests," *Geotextiles and Geomembranes*, vol. 19, no. 4, pp. 195–212, 2001.

[25] G. M. Filz and J. J. B. Esterhuizen, "Progressive failure of lined waste impoundmen," *Journal of Geotechnical and Geoenvironmental Engineering*, vol. 127, no. 10, pp. 841–848, 2001.

[26] H. H. Zhu, C. C. Zhang, and C. S. Tang, "Modeling the pullout behavior of short fiber in reinforced," *Geotextiles and Geomembranes*, vol. 42, no. 4, pp. 329–338, 2014.

[27] C. C. Zhang, H. H. Zhu, and C. S. Tang, "Modeling of progressive interface failure of fiber reinforced soil," *Journal of Zhejiang University*, vol. 49, no. 10, pp. 1952–1959, 2015.

[28] L. P. Li, F. W. Lai, and F. Q. Chen, "Simple analysis solution to predict progressive pullout behavior of geosynthetics in

reinforced soil," *Nonferrous Metals*, vol. 68, no. 4, pp. 74–80, 2016.

[29] H. Cheng, X. Wang, and J. S. Zhang, "Shear behavior of geogrid-soil interface and its statistical damage softening model," *Journal of Railway Science and Engineering*, vol. 15, no. 11, pp. 2780–2787, 2018.

[30] The Professional Standards Compilation Group of People′s Republic of China, *JTG E50-2006 Test Methods of Geosynthetics for Highway Engineering*, China Communications Press, Beijing, China, 2006.

[31] J. Lemaitre, *A Course on Damage Mechanics*, Spring-Verlag, New York, NY, USA, 1992.

[32] R. Walpole and R. Myers, *Probability and Statistics for Engineers and Scientists*, Academic Press, San Diego, CA, USA, 2014.